Diffractive heavy vector meson production from the BFKL equation

R. Enberg[1], L. Motyka[1,3], G. Poludniowski[2]

[1] Department of Radiation Sciences, Uppsala University, Box 535, 751 21 Uppsala, Sweden
[2] Department of Physics and Astronomy, University of Manchester, Manchester M13 9PL, UK
[3] Institute of Physics, Jagellonian University, Reymonta 4, 30-059 Kraków, Poland

Abstract. Diffractive heavy vector meson photoproduction accompanied by proton dissociation is studied for arbitrary momentum transfer. The process is described by the non-forward BFKL equation, for which a complete analytical solution is found, giving the scattering amplitude. The impact of non-leading corrections to the BFKL equation is also analysed. Results are compared to the HERA data on J/ψ production.

1 Introduction

Quantum Chromodynamics offers unique opportunities to study the richness of dynamical phenomena of nonlinear quantum field theory. One of the most interesting problems is related to the colour flow in high energy scattering. In particular, diffractive processes correspond to an exchange of a colour singlet system of quarks and gluons between scattering objects. Such diffractive phenomena possess a very clean experimental signature, namely a large rapidity interval devoid of particles (i.e. a rapidity gap).

The perturbative QCD description of the hard colour singlet exchange across a large rapidity interval y relies on the Balitsky-Fadin-Kuraev-Lipatov (BFKL) equation [1, 2]. In this framework, the leading powers of rapidity in the perturbative expansion are resummed, giving the amplitude for hard pomeron exchange. The pomeron is viewed as a composite system of two reggeized gluons in the colour singlet state. The status of the BFKL approach to QCD amplitudes is still under discussion, and both theoretical improvements and experimental tests are necessary.

Diffractive photoproduction of a heavy vector meson, separated from the proton remnant by a large rapidity gap has been proposed [3,4] as an ideal probe of the BFKL pomeron, see Fig. 1. Indeed, this process permits detailed studies of both the momentum transfer and the rapidity dependence of the scattering amplitude. The vector meson mass and the momentum transfer t provide the hard scale required for the perturbative treatment of QCD processes, and the sensitivity to the infra-red region is small, contrary to the case of inclusive hard diffraction.

There are some very recent measurements of this process from HERA [5] that allow the theoretical models to be tested. The available calculations [3,4,6] of the cross-sections for heavy vector meson production are based on the Mueller-Tang approximation [7] to the solution of the leading logarithmic BFKL equation. In this approximation, parts of the amplitude which vanish in the limit $y \to \infty$ are neglected [8,4].

Recently, it has been shown [6] that fitting these results to the data, one obtains a good quantitative agreement with the differential cross-section. Still, the important non-leading corrections to the BFKL kernel [9] are not accounted for. Furthermore, the Mueller-Tang approximation is only good for very large rapidities, and may need improvement in order to understand the experimental data. Indeed, it has been found that to describe the events with gaps between jets subleading corrections to the Mueller-Tang picture are important [8,10].

Thus, the main goal of this paper is to investigate diffractive heavy[1] vector meson photoproduction beyond the leading logarithmic BFKL equation and beyond the Mueller-Tang approximation. The obtained results are compared to previous ones [3,4] and to the experimental data from HERA [5]. In Sect. 2 we define the framework, in Sect. 3 the BFKL equation is presented, and in Sect. 4 an exact solution of the equation is derived. Properties of the exact and numerical solutions are studied in Sect. 5, comparison with data is performed in Sect. 6, and in Sect. 7 conclusions are given.

2 Hard colour singlet exchange

The diffractive process $\gamma p \to V X$ at large momentum transfer t (see Fig. 1) takes place by exchange of the BFKL

---

[1] Light vector meson production will be studied in a forthcoming paper [11]
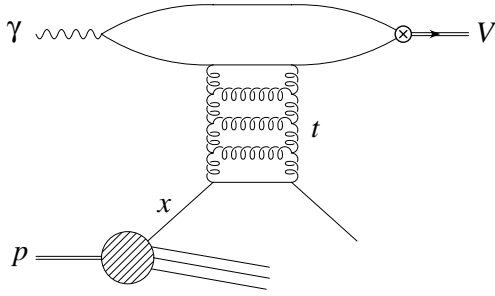
Fig. 1. Feynman diagram illustrating vector meson photoproduction at high momentum transfer

pomeron. It has been demonstrated, that at large momentum transfer, the hard pomeron couples predominantly to individual partons in the proton [12]. Thus, the cross-section may be factorized into a product of the parton level cross-section and the parton distribution functions,

$$\frac{d\sigma(\gamma p \to VX)}{dt\,dx_j}$$

$$= \left(\frac{4N_c^4}{(N_c^2-1)^2}G(x_j,t) + \sum_f[q_f(x_j,t) + \bar{q}_f(x_j,t)]\right)$$

$$\times \frac{d\sigma(\gamma q \to Vq)}{dt}, \tag{1}$$

where $N_c = 3$, $G(x_j,t)$ and $q_f(x_j,t)$ are the gluon and quark distribution functions respectively, and W^2 is the γp centre-of-mass energy squared. The struck parton in the proton, initiating a jet in the proton hemisphere, carries the fraction x_j of the longitudinal momentum of the incoming proton. The partonic cross-section, characterized by the invariant collision energy squared $\hat{s} = x_j W^2$ is expressed in terms of the amplitude $\mathcal{A}(\hat{s},t)$,

$$\frac{d\sigma}{dt} = \frac{1}{16\pi}|\mathcal{A}(\hat{s},t)|^2. \tag{2}$$

The amplitude is dominated by its imaginary part, which we shall parametrize, as in [3,6], by a dimensionless quantity $\mathcal{F}$

$$\mathcal{I}m\,\mathcal{A}(\hat{s},t) = \frac{16\pi}{9t^2}\mathcal{F}(z,\tau) \tag{3}$$

where z and τ are defined by

$$z = \frac{3\alpha_s}{2\pi}\ln\left(\frac{\hat{s}}{\Lambda^2}\right) \tag{4}$$

$$\tau = \frac{|t|}{M_V^2 + Q_\gamma^2}, \tag{5}$$

where M_V is the mass of the vector meson, Q_γ is the photon virtuality[2] and Λ^2 is a characteristic mass scale related to M_V^2 and $|t|$. Following the results of [6] we assume $\Lambda^2 = M_V^2 + Q_\gamma^2$. For completeness, we give the cross-section expressed in terms of $\mathcal{F}(z,\tau)$, where the real part of the amplitude is neglected,

---

[2] In this paper we only consider $Q_\gamma = 0$

$$\frac{d\sigma(\gamma q \to Vq)}{dt} = \frac{16\pi}{81t^4}|\mathcal{F}(z,\tau)|^2. \tag{6}$$

This representation is rather convenient for the calculations performed in Sect. 4.

3 The BFKL equation

The imaginary part $\mathcal{I}m\,A(\hat{s},t)$ of the amplitude for the process $\gamma p \to V + \text{gap} + X + \text{jet}$ corresponds to the diagram in Fig. 1 illustrating QCD pomeron exchange, and can be written in the following form:

$$\mathcal{I}m\,\mathcal{A}(\hat{s},t=-q^2)$$

$$= \int \frac{d^2\boldsymbol{k}}{\pi}\frac{\Phi^0_{\gamma V}(k^2,q^2)\Phi_{qq}(x,\boldsymbol{k},\boldsymbol{q})}{[(\boldsymbol{k}+\boldsymbol{q}/2)^2+s_0][(\boldsymbol{k}-\boldsymbol{q}/2)^2+s_0]}. \tag{7}$$

In this equation, x is the longitudinal momentum fraction of the incoming proton taken by the hard pomeron, $x = \Lambda^2/\hat{s}$, $\boldsymbol{q}/2 \pm \boldsymbol{k}$ denote the transverse momenta of the exchanged gluons, and $\boldsymbol{q}$ is the transverse part of the momentum transfer. In the propagators corresponding to the exchanged gluons we include the parameter s_0 which can be viewed as the effective representation of the inverse of the colour confinement radius squared. Investigation of such non-perturbative effects in the gluon propagator at low virtualities was performed, for instance, in [13], where it was found that $0.1\,\text{GeV}^2 < s_0 < 0.5\,\text{GeV}^2$. Recent lattice studies [14] indicate a value of s_0 between $0.25\,\text{GeV}^2$ and $0.65\,\text{GeV}^2$. Having some freedom here, we choose $s_0 = 0.5\,\text{GeV}^2$. The sensitivity of the cross-section to the magnitude of s_0 can serve as an estimate of the sensitivity of the results to the contribution coming from the infra-red region. It should be noted that formula (7) gives a finite result in the limit $s_0 = 0\,\text{GeV}^2$. An interesting discussion of non-perturbative effects in the gluon propagator in the context of vector meson production can be found in [15].

The couplings of the external particle pair to the colour singlet gluonic ladder are described, in the high energy limit, by impact factors $\Phi^0_{\gamma V}(k^2,q^2)$ and $\Phi^0_{qq}(k^2,q^2)$ for the $\gamma \to V$ transition and the quark elastic scattering, respectively. The impact factors are obtained in the perturbative QCD framework and we approximate them by the leading terms in the perturbative expansion [16]:

$$\Phi^0_{\gamma V} = \frac{\mathcal{C}\alpha_s}{2}\left(\frac{1}{\bar{q}^2} - \frac{1}{q_\parallel^2 + k^2}\right),$$

$$\Phi^0_{qq} = \alpha_s. \tag{8}$$

In the former formula, factorization of the scattering process and the meson formation is assumed, and the non-relativistic approximation of the meson wave function is used. In this approximation the quarks in the meson have collinear four-momenta and $M_V = 2M_q$ where M_q is the mass of the constituent quark. To leading order accuracy, the constant $\mathcal{C}$ may be related to the vector meson leptonic decay width

$$\mathcal{C}^2 = \frac{3\Gamma_{ee}^V M_V^3}{\alpha}. \tag{9}$$

We have also defined

$$\bar{q}^2 = q_\parallel^2 + q^2/4, \tag{10}$$

$$q_\parallel^2 = (Q_\gamma^2 + M_V^2)/4. \tag{11}$$

This standard approximation is based on the fact, that the typical quark three-momenta in charmonium states are much smaller than the charm quark mass. Still, these momenta are non-zero, leading to a smearing of the non-relativistic form-factor. The resulting corrections were extensively discussed e.g. in [17] for the forward scattering case. Moreover, it is expected at larger momentum transfer $|t| > M_V^2$, that the relativistic effects become enhanced, as the mass is no longer the largest scale in the process. For instance, in the non-relativistic approximation one neglects helicity flip processes, whose relative contribution may grow with increasing momentum transfer, as was demonstrated for a single helicity flip amplitude for light vector mesons [18]. Therefore, the applied approximation may be inaccurate at very large momentum transfers.

The function $\Phi_{qq}(x, \mathbf{k}, \mathbf{q})$ satisfies the BFKL equation, which in the leading $\ln(1/x)$ approximation has the following form:

$$
\begin{aligned}
&\Phi_{qq}(x, \mathbf{k}, \mathbf{q}) \\
&= \Phi_{qq}^0(k^2, q^2) + \frac{3\alpha_s}{2\pi^2} \int_x^1 \frac{dx'}{x'} \int \frac{d^2\mathbf{k}'}{(\mathbf{k}' - \mathbf{k})^2 + s_0} \\
&\times \left\{ \left[\frac{\mathbf{k}_1^2}{\mathbf{k}_1'^2 + s_0} + \frac{\mathbf{k}_2^2}{\mathbf{k}_2'^2 + s_0} - q^2 \frac{(\mathbf{k}' - \mathbf{k})^2 + s_0}{(\mathbf{k}_1'^2 + s_0)(\mathbf{k}_2'^2 + s_0)} \right] \right. \\
&\times \Phi_{qq}(x', \mathbf{k}', \mathbf{q}) \\
&- \left[\frac{\mathbf{k}_1^2}{\mathbf{k}_1'^2 + (\mathbf{k}' - \mathbf{k})^2 + 2s_0} + \frac{\mathbf{k}_2^2}{\mathbf{k}_2'^2 + (\mathbf{k}' - \mathbf{k})^2 + 2s_0} \right] \\
&\left. \times \Phi_{qq}(x', \mathbf{k}, \mathbf{q}) \right\} \tag{12}
\end{aligned}
$$

where

$$\mathbf{k}_{1,2} = \frac{\mathbf{q}}{2} \pm \mathbf{k}, \qquad \mathbf{k}'_{1,2} = \frac{\mathbf{q}}{2} \pm \mathbf{k}' \tag{13}$$

denote the transverse momenta of the gluons. At leading logarithmic accuracy, a fixed value of the QCD coupling α_s should be used in equations (8) and (12).

It is known that the BFKL equation can acquire significant non-leading contributions [9]. Although the structure of those corrections is fairly complicated, their dominant part is rather simple, and follows from restricting the integration region in the real emission term in (12) [19,20]. For $q = 0$ the relevant limitation is [19,21]

$$k'^2 \leq k^2 \frac{x'}{x}. \tag{14}$$

This follows from the requirement that the virtuality of the gluons exchanged along the chain is dominated by the transverse momentum squared. The constraint (14) can be shown to exhaust about 70% of the next-to-leading corrections to the QCD pomeron intercept [9,19]. Generalization

of the constraint (14) to the case of a non-forward configuration with $q^2 \geq 0$ is assumed to take the following form [22,10]:

$$k'^2 \leq (k^2 + q^2/4) \frac{x'}{x}. \tag{15}$$

The latter formula gives at $k^2 < q^2/4$ a less restrictive relation for k' in respect to k, than constraint (14) in the forward case. Consequently, the generalized constraint (15) may realize, at larger momentum transfer, a smaller fraction of the non-leading corrections than the quoted 70% at $q^2 = 0$. This would mean that our estimate of the cross-section could be too high at larger q^2.

Another important part of the non-leading corrections to the BFKL equation is related to running of the coupling constant within the ladder. To be consistent, the running coupling will also be used in the impact factors (8). Besides the BFKL equation (12) in the leading logarithmic approximation we shall therefore also consider the equation embodying the constraint (15) and a running coupling in order to estimate the effects of the non-leading contributions.

The corresponding equation which contains constraint (15) in the real emission term reads:

$$
\begin{aligned}
&\Phi_{qq}(x, \mathbf{k}, \mathbf{q}) \\
&= \Phi_{qq}^0(k^2, q^2) + \frac{3\alpha_s(\mu^2)}{2\pi^2} \int_x^1 \frac{dx'}{x'} \int \frac{d^2\mathbf{k}'}{(\mathbf{k}' - \mathbf{k})^2 + s_0} \\
&\times \left\{ \left[\frac{\mathbf{k}_1^2}{\mathbf{k}_1'^2 + s_0} + \frac{\mathbf{k}_2^2}{\mathbf{k}_2'^2 + s_0} - q^2 \frac{(\mathbf{k}' - \mathbf{k})^2 + s_0}{(\mathbf{k}_1'^2 + s_0)(\mathbf{k}_2'^2 + s_0)} \right] \right. \\
&\times \Phi_{qq}(x', \mathbf{k}', \mathbf{q}) \Theta \left((k^2 + q^2/4)x'/x - k'^2 \right) \\
&- \left[\frac{\mathbf{k}_1^2}{\mathbf{k}_1'^2 + (\mathbf{k}' - \mathbf{k})^2 + 2s_0} + \frac{\mathbf{k}_2^2}{\mathbf{k}_2'^2 + (\mathbf{k}' - \mathbf{k})^2 + 2s_0} \right] \\
&\left. \times \Phi_{qq}(x', \mathbf{k}, \mathbf{q}) \right\}. \tag{16}
\end{aligned}
$$

with the scale of the coupling set to $\mu^2 = k^2 + q^2/4 + s_0$. The scales of the coupling constants in the impact factors should be related to the virtualities entering the vertices. A natural choice is then

$$
\begin{aligned}
\mu_1^2 &= k^2 + M_c^2 &&\text{in} &&\Phi_{\gamma V}^0, \\
\mu_2^2 &= k^2 + s_0 &&\text{in} &&\Phi_{qq}^0, \tag{17}
\end{aligned}
$$

with k^2 being the virtuality of the gluon entering the vertex. We will also consider another choice

$$\mu_1'^{\,2} = \mu_1^2/4 \quad\text{and}\quad \mu_2'^{\,2} = \mu_2^2/4, \tag{18}$$

necessary in order to obtain a good fit to the data. A similar choice of scales was needed to describe double-tagged events at LEP in an analogous NL-BFKL framework [23]. Equations (12) and (16) are solved using an approximate numerical technique, described in detail in [22] and [10].

4 The exact LL BFKL solution

The BFKL kernel (12) in the leading logarithmic approximation exhibits, in the impact parameter representation, invariance under conformal transformations [2]. The conformal symmetry of the kernel permits the following expansion of the amplitude in the basis of eigenfunctions $E_{n,\nu}$ [2]:

$$
\mathcal{F}(z,\tau) = \frac{t^2}{(2\pi)^3} \sum_{n=-\infty}^{n=\infty} \int_{-\infty}^{\infty} d\nu
$$

$$
\times \frac{\nu^2 + n^2/4}{[\nu^2 + (n-1)^2/4][\nu^2 + (n+1)^2/4]}
$$

$$
\times \exp[\chi_n(\nu)z] \, I_{n,\nu}^A(q) \, (I_{n,\nu}^B(q))^* \qquad (19)
$$

where

$$
\chi_n(\nu) = 4\mathcal{R}e\left(\psi(1) - \psi(1/2 + |n|/2 + i\nu) \right) \qquad (20)
$$

is proportional to the eigenvalues of the BFKL kernel and

$$
I_{n,\nu}^A(q) = \int \frac{d^2k}{(2\pi)^2} \mathcal{I}_A(k,q) \int d^2\rho_1 \, d^2\rho_2 \, E_{n,\nu}(\rho_1,\rho_2)
$$

$$
\times \exp(ik\cdot\rho_1 + i(q-k)\cdot\rho_2) \qquad (21)
$$

(and analogously for the index B). The eigenfunctions are given by

$$
E_{n,\nu}(\rho_1,\rho_2) = \left(\frac{\rho_1 - \rho_2}{\rho_1\rho_2} \right)^h \left(\left(\frac{\rho_1 - \rho_2}{\rho_1\rho_2} \right)^* \right)^{\tilde{h}} \qquad (22)
$$

where $h = 1/2 + n/2 + i\nu$ and $\tilde{h} = 1/2 - n/2 + i\nu$. Here k and q are transverse two dimensional momentum vectors, and ρ_1 and ρ_2 are position space vectors in the standard complex representation (e.g. $k = k_x + ik_y$). The scalar product in this representation is given by, e.g., $k \cdot \rho_1 = k^*\rho_1/2 + k\rho_1^*/2$. The functions $\mathcal{I}_A = \Phi_{\gamma V}^0$ and $\mathcal{I}_B = \Phi_{qq}^0$ are the impact factors (8).

The quark impact factor in representation (21) was found in [8], generalizing the Mueller-Tang subtraction [7] to non-zero conformal spin;

$$
I_{n,\nu}^{qq}(q) = -\frac{4\pi \alpha_s i^n}{|q|} \left(\frac{|q|^2}{4} \right)^{i\nu} \left(\frac{q^*}{q} \right)^{n/2}
$$

$$
\times \frac{\Gamma(1/2 + n/2 - i\nu)}{\Gamma(1/2 + n/2 + i\nu)} \qquad (23)
$$

for even n and $I_{n,\nu}^{qq} = 0$ for odd n.

The impact factor for the $\gamma \to V$ transition is known for $n = 0$ [4]. We shall generalize this result to arbitrary n, which requires evaluating the following integrals

$$
I_{n,\nu}^{\gamma V}(q) = \int \frac{d^2k}{(2\pi)^2} \mathcal{I}_{\gamma V}(k,q) \int d^2\rho_1 \, d^2\rho_2 \, E_{n,\nu}(\rho_1,\rho_2)
$$

$$
\times \exp\left(ik^*\rho_1/2 + ik\rho_1^*/2 \right.
$$

$$
\left. +i(q^* - k^*)\rho_2/2 + i(q-k)\rho_2^*/2 \right). \qquad (24)
$$

Changing variables to $\rho_1 = R + \rho/2$, $\rho_2 = R - \rho/2$ and integrating over d^2k we get

$$
I_{n,\nu}^{\gamma V}(q) = -\frac{\mathcal{C}\,\alpha_s}{4\pi} \int d^2\rho \, K_0(q_\parallel|\rho|)
$$

$$
\times \int d^2R \, E_{n,\nu}(R + \rho/2, R - \rho/2)
$$

$$
\times \exp(iq^*R/2 + iqR^*/2). \qquad (25)
$$

The integral over d^2R was obtained by Navelet and Peschanski [24]. Inserting their result one obtains

$$
I_{n,\nu}^{\gamma V}(q) = -\frac{\mathcal{C}\,\alpha_s}{4\pi} \int d^2\rho \, \frac{(-1)^n|\rho|}{2\pi^2} \, b_{n,\nu} \, \hat{E}_{n,\mu}(\rho, \rho^*)
$$

$$
\times K_0(q_\parallel|\rho|) \qquad (26)
$$

where

$$
\hat{E}_{n,\mu}(\rho, \rho^*) = \left(\frac{|q|}{8} \right)^{2i\nu} \left(\frac{q^*}{q} \right)^{n/2} \qquad (27)
$$

$$
\times \Gamma(1 - i\nu + n/2) \, \Gamma(1 - i\nu - n/2)
$$

$$
\times \left[J_{n/2-i\nu}(q^*\rho/4) \, J_{-n/2-i\nu}(q\rho^*/4) \right.
$$

$$
\left. - (-1)^n \, J_{-n/2+i\nu}(q^*\rho/4) \, J_{n/2+i\nu}(q\rho^*/4) \right]
$$

and

$$
b_{n,\nu} = \frac{2^{4i\nu}\pi^3}{|n|/2 - i\nu} \frac{\Gamma(|n|/2 - i\nu + 1/2)\Gamma(|n|/2 + i\nu)}{\Gamma(|n|/2 + i\nu + 1/2)\Gamma(|n|/2 - i\nu)}. \qquad (28)
$$

Thus, we have a result in terms of a double integral over $d^2\rho = |\rho| \, d|\rho| \, d\phi$. Further, we represent the Bessel functions by their power series expansions $J_\sigma(z) = (z/2)^\sigma \sum_{k=0}^{\infty} (-1)^k (z/2)^{2k}/[\Gamma(k+1)\Gamma(\sigma+k+1)]$ and obtain

$$
J_{n/2-i\nu}(q^*\rho/4) \, J_{-n/2-i\nu}(q\rho^*/4) \qquad (29)
$$

$$
- (-1)^n \, J_{-n/2+i\nu}(q^*\rho/4) \, J_{n/2+i\nu}(q\rho^*/4)
$$

$$
= \left[\sum_{k=0}^{\infty} \sum_{l=0}^{\infty} \left\{ \left((-1)^{k+l} \, (|q||\rho|/8)^{2k+2l-2i\nu} \right. \right.\right.
$$

$$
\times \exp[i\phi(2l - 2k + n)] \Big) \Big/ \Big(\Gamma(k+1) \, \Gamma(l+1)
$$

$$
\left.\left.\left. \times \Gamma(1 + l + n/2 - i\nu) \, \Gamma(1 + k - n/2 - i\nu) \right) \right\} \right] - [c.c.].
$$

Both the ϕ and $|\rho|$ integrations in (25) are performed term by term in the sums (29). All the ϕ dependence of the integrand in (25) is due to expression (29) where in the subsequent terms only integer powers of $\exp(i\phi)$ appear. Thus, after the angular integration, only terms with $n + 2k - 2l = 0$ contribute, and one of the summations in (29) may be trivially performed giving

$$
\int_0^{2\pi} d\phi \left[J_{n/2-i\nu}(q^*\rho/4) \, J_{-n/2-i\nu}(q\rho^*/4) \right.
$$

$$- (-1)^n \, J_{-n/2+i\nu}(q^*\rho/4) \, J_{n/2+i\nu}(q\rho^*/4) \Bigg]$$

$$= \Bigg[2\pi \sum_{l=0}^{\infty} \Bigg\{ \Big((-1)^{|n|/2} \, (|q||\rho|/8)^{4l+|n|-2i\nu} \Big)$$

$$\Big/ \Big(\Gamma(1+l) \, \Gamma(1+l+|n|/2) \, \Gamma(1+l-i\nu)$$

$$\times \Gamma(1+l+|n|/2-i\nu) \Big) \Bigg\} \Bigg] - [c.c.]. \qquad (30)$$

Note that the odd n contributions are all zero. Using (30) and performing the remaining $|\rho|$ integration in (25), we have

$$\int_0^{\infty} d|\rho| \, |\rho|^2 \, K_0(q_\|\,|\rho|) \int_0^{2\pi} d\phi$$

$$\times \Bigg[J_{n/2-i\nu}(q^*\rho/4) \, J_{-n/2-i\nu}(q\rho^*/4)$$

$$- (-1)^n \, J_{-n/2+i\nu}(q^*\rho/4) \, J_{n/2+i\nu}(q\rho^*/4) \Bigg]$$

$$= \Bigg[\frac{4\pi}{q_\|^3} \sum_{l=0}^{\infty} \Bigg\{ \Big((-1)^{|n|/2} \, \Gamma^2(3/2 - i\nu + 2l + |n|/2)$$

$$\times (|q|/4q_\|)^{4l+|n|-2i\nu} \Big) \Big/ \Big(\Gamma(1+l) \, \Gamma(1+l+|n|/2)$$

$$\times \Gamma(1+l-i\nu) \Gamma(1+l+|n|/2-i\nu) \Big) \Bigg\} \Bigg] - [c.c.]. \quad (31)$$

The obtained series is convergent for $|q|/4q_\| < 1$, where the infinite sum gives the value of the integral. We need to continue analytically the result to $|q|/4q_\| \geq 1$. Thus, we represent this infinite sum of terms $\mathcal{A}(l)$ as an integral over complex l using a Sommerfeld-Watson type transform. A contour $\mathcal{C}_1$ in the complex l plane is introduced enclosing the half-plane $\mathcal{R}e\,(l) > -1/2$ where $\mathcal{A}(l)$ has no poles. It is possible to construct a function $\mathcal{D}(l)$ with a pole structure and with residues such that the contour integral of $\mathcal{D}(l)\mathcal{A}(l)/(2\pi i)$ along $\mathcal{C}_1$, evaluated using the Cauchy theorem, reproduces the initial sum over the index l. It is easy to verify that

$$\mathcal{D}(l) = -\pi \frac{\sin \pi i\nu}{\sin \pi l \, \sin \pi(l - i\nu)}$$

$$= \frac{\Gamma(l)\Gamma(1-l)\Gamma(l-i\nu)\Gamma(1-l+i\nu)}{\Gamma(i\nu)\Gamma(1-i\nu)} \qquad (32)$$

has the desired properties. Thus one has

$$\Bigg[\frac{4\pi}{q_\|^3} \sum_{l=0}^{\infty} \Bigg\{ \Big((-1)^{|n|/2} \, \Gamma^2(3/2 - i\nu + 2l + |n|/2)$$

$$\times (|q|/4q_\|)^{4l+|n|-2i\nu} \Big) \Big/ \Big(\Gamma(1+l) \, \Gamma(1+l+|n|/2)$$

$$\times \Gamma(1+l-i\nu) \, \Gamma(1+l+|n|/2-i\nu) \Big) \Bigg\} \Bigg] - [c.c.]$$

$$= \frac{4\pi}{q_\|^3} \oint_{\mathcal{C}_1} \frac{dl \, \mathcal{D}(l)}{2\pi i} \Bigg\{ \Big((-1)^{|n|/2} \, (|q|/4q_\|)^{4l+|n|-2i\nu}$$

$$\times \Gamma^2(3/2 - i\nu + 2l + |n|/2) \Big)$$

$$\Big/ \Big(\Gamma(1+l) \, \Gamma(1+l+|n|/2)$$

$$\times \Gamma(1+l-i\nu) \, \Gamma(1+l+|n|/2-i\nu) \Big) \Bigg\}. \qquad (33)$$

The contribution from the region of complex $l \to \infty$ vanishes in the limit, so the value of the contour integral is given by a line integral

$$\Bigg[\frac{4\pi}{q_\|^3} \sum_{l=0}^{\infty} \Bigg\{ \Big((-1)^{|n|/2} \, \Gamma^2(3/2 - i\nu + 2l + |n|/2)$$

$$\times (|q|/4q_\|)^{4l+|n|-2i\nu} \Big) \Big/ \Big(\Gamma(1+l) \, \Gamma(1+l+|n|/2)$$

$$\times \Gamma(1+l-i\nu) \, \Gamma(1+l+|n|/2-i\nu) \Big) \Bigg\} \Bigg] - [c.c.]$$

$$= -\frac{4\pi}{q_\|^3} (-1)^{|n|/2} \int_{-1/2-i\infty}^{-1/2+i\infty} \frac{dl}{2\pi i} \, (|q|/4q_\|)^{4l+|n|-2i\nu}$$

$$\times \frac{\Gamma(l-i\nu) \, \Gamma(1-l+i\nu)}{\Gamma(i\nu) \, \Gamma(1-i\nu)} \frac{\Gamma(l) \, \Gamma(1-l)}{\Gamma(1+l) \, \Gamma(1+l-i\nu)}$$

$$\times \frac{\Gamma^2(3/2 + 2l + |n|/2 - i\nu)}{\Gamma(1+l+|n|/2) \, \Gamma(1+l+|n|/2-i\nu)}. \qquad (34)$$

This form is suggestive of the $n = 0$ result of [4]. Substituting $s = 2l + 1 - i\nu$, $\tau = q^2/4q_\|^2$ and using the Euler Γ-function relations such as the doubling formula $2^{2z-1}\Gamma(z)\Gamma(z + 1/2) = \sqrt{\pi}\,\Gamma(2z)$ allows simplification of the integrand. Inserting (27) and (28) into (26), taking into account (34) and using the identity $(-1)^{|n|/2} \frac{\Gamma(i\nu+|n|/2)\,\Gamma(1-i\nu-|n|/2)}{\Gamma(i\nu)\,\Gamma(1-i\nu)} = 1$ for even n, we obtain the final answer,

$$I_{n,\nu}^{\gamma V}(q) = \mathcal{C} \, \alpha_s \, \frac{8\pi^2}{|q|^3} \left(\frac{|q|^2}{4} \right)^{i\nu} \left(\frac{q^*}{q} \right)^{n/2} \left(\frac{1}{4} \right)^{|n|/2}$$

$$\times \frac{\Gamma(1/2 - i\nu + |n|/2)}{\Gamma(1/2 + i\nu + |n|/2)}$$

$$\times \int_{-i\infty}^{i\infty} \frac{ds}{2\pi i} \, \tau^{1/2+s+|n|/2}$$

$$\times \frac{\Gamma(1 - s - i\nu) \, \Gamma(1 - s + i\nu)}{\Gamma(1 - s/2 - i\nu/2) \, \Gamma(1 - s/2 + i\nu/2)}$$

$$\times \Bigg\{ \Big(\Gamma^2(1/2 + s + |n|/2) \Big)$$

$$\Big/ \Big(\Gamma(1/2 + s/2 - i\nu/2 + |n|/2)$$

$$\times \Gamma(1/2 + s/2 + i\nu/2 + |n|/2) \Big) \Bigg\} \qquad (35)$$

for even n and $I_{n,\nu}^{\gamma V} = 0$ for odd n. This agrees with the corresponding expression of Bartels et al. for $n = 0$ [4]. The r.h.s. of (35) is the desired analytic continuation of the sum of the infinite power series (c.f. (31)) which holds for all values of τ. Introducing the notation $m = n/2$, and using the result for $I_{n,\nu}^{qq}$, we arrive at the amplitude

$$\mathcal{F}(z,\tau) = 4\mathcal{C}\,\alpha_s^2 \sum_{m=-\infty}^{m=\infty} \left(-\frac{1}{4}\right)^{|m|} \tag{36}$$

$$\times \int d\nu \, \frac{\nu^2 + m^2}{(\nu^2 + (m-1/2)^2)(\nu^2 + (m+1/2)^2)} \, e^{\chi_m(\nu)z}$$

$$\times \int_{-i\infty}^{i\infty} \frac{ds}{2\pi i} \, \tau^{1/2 + s + |m|}$$

$$\times \frac{\Gamma(1-s-i\nu)\,\Gamma(1-s+i\nu)}{\Gamma(1-s/2-i\nu/2)\,\Gamma(1-s/2+i\nu/2)}$$

$$\times \frac{\Gamma^2(1/2+s+|m|)}{\Gamma(1/2+s/2-i\nu/2+|m|)\,\Gamma(1/2+s/2+i\nu/2+|m|)},$$

which is equal to

$$\mathcal{F}(z,\tau) = \frac{8\mathcal{C}\,\alpha_s^2}{\pi} \sum_{m=-\infty}^{m=\infty} (-1)^m$$

$$\times \int d\nu \, \frac{\nu^2 + m^2}{(\nu^2 + (m-1/2)^2)(\nu^2 + (m+1/2)^2)} \, e^{\chi_m(\nu)z}$$

$$\times \int_{-i\infty}^{i\infty} \frac{ds}{2\pi i} \left(\frac{\tau}{4}\right)^{1/2+s+|m|} \left\{ \left(\Gamma(1/2-s/2+i\nu/2)\right.\right.$$

$$\times \Gamma^2(1/2+s+|m|)\,\Gamma(1/2-s/2-i\nu/2)\Big)$$

$$\Big/ \Big(\Gamma(1/2+s/2-i\nu/2+|m|)$$

$$\times \Gamma(1/2+s/2+i\nu/2+|m|)\Big) \Big\}. \tag{37}$$

Note that the m contribution is equal to the $-m$ contribution.

5 Properties of the solutions

The form of the solution to the BFKL equation given by (37) is simple enough to perform extended studies of the amplitude, including the impact of higher conformal spins. The remaining complex integrations over s and ν are performed numerically. In the analysis we take the real photon case, $Q_\gamma^2 = 0$. First, we set $z = 0$ in which case the LO BFKL amplitude is described by a simple two-gluon exchange,

$$\mathcal{F}(z=0,\tau) = \mathcal{C}\,\alpha_s^2 \left(\frac{4\tau^2}{1-\tau^2}\right) \ln\left(\frac{(1+\tau)^2}{4\tau}\right). \tag{38}$$

A valuable cross check of our calculation is to investigate how the two-gluon exchange amplitude builds up when subsequent higher conformal spin components are being added. In Fig. 2 we show curves corresponding to $|\mathcal{F}(z,\tau)/(\mathcal{C}\,\alpha_s)|^2$ approximated by partial sums over m in (37) up to $m = m_{\max} = 0, 1, 4$ and compare them with the amplitude given by (38). It is clear that results coming from the two approaches agree. The sum over conformal spins converges quickly to the exact result, however more terms are needed for increasing τ. Note, that the $m = n = 0$ component and the exact result have about
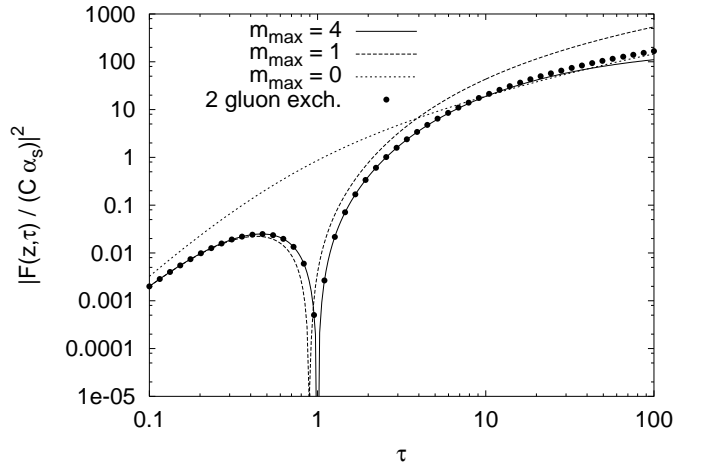

Fig. 2. The amplitude squared for the diffractive heavy vector meson production off a quark at zero rapidity ($z = 0$): the exact two-gluon exchange result (dots) compared with sums of contributions up to conformal spin $n_{\max} = 2m_{\max}$ (lines)

the same absolute values for $\tau \gg 1$ but the signs of the amplitudes are opposite.

Having checked this, we are in a position to study the importance of higher conformal spins at $z > 0$. Thus, in Fig. 3 the ratio of $\mathcal{F}(z,\tau)$ (with $m_{\max} = 7$) to the $m = 0$ component is plotted for various z as a function of τ and for various τ as a function of z. The relative importance of the higher conformal spins for the cross-section may be read out from Fig. 4. The contours show constant values of

$$\mathcal{E} = \frac{d\sigma/dt|_{\text{exact}} - d\sigma/dt|_{n=0}}{d\sigma/dt|_{n=0}}, \tag{39}$$

giving therefore the relative error of the conventional leading conformal spin approximation in the (z, τ) plane. As expected, the correction due to $m \neq 0$ components decreases with increasing z (or y) and increases with increasing τ (or $|t|$). Note also the line $d\sigma/dt = 0$ on which the complete amplitude changes sign, leading to a dip in the cross-section $d\sigma/dt|_{\text{exact}}$. Such a dip does not appear in the leading conformal spin approximation.

The analytical results may also be used to test the method and approximations used in the numerical approach to the non-forward BFKL equation [22,10]. In Fig. 5, a comparison between results obtained in these two frameworks is given. With good accuracy the numerical solution coincides with the analytical one. At larger values of z and τ a discrepancy between the two solutions appears. This is caused by an upper cut-off $K_F = 10^5$ GeV imposed on the gluon transverse momenta, which is necessary for the numerical approach. The very large gluon momenta that are affected by this procedure contribute significantly to the amplitudes when the momentum transfer and/or the rapidity is very large.

The non-leading corrections [9] to the BFKL equation have a large impact on the rapidity dependence of the cross-sections, as already discussed. At high rapidities, this leads to dramatic effects in the magnitude of the cross-section [22]. Therefore it is important to incorporate
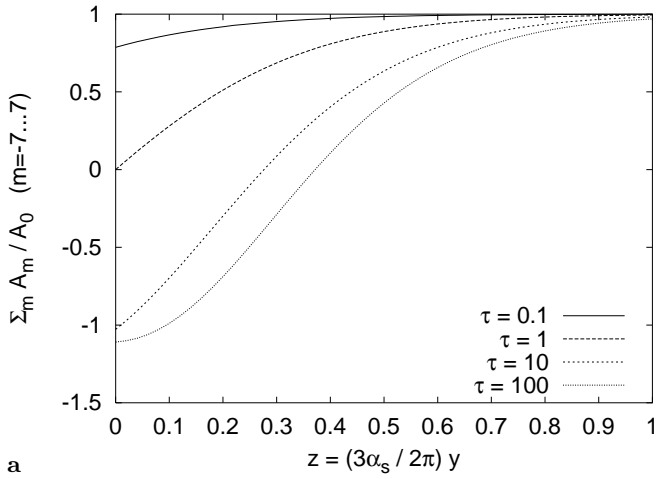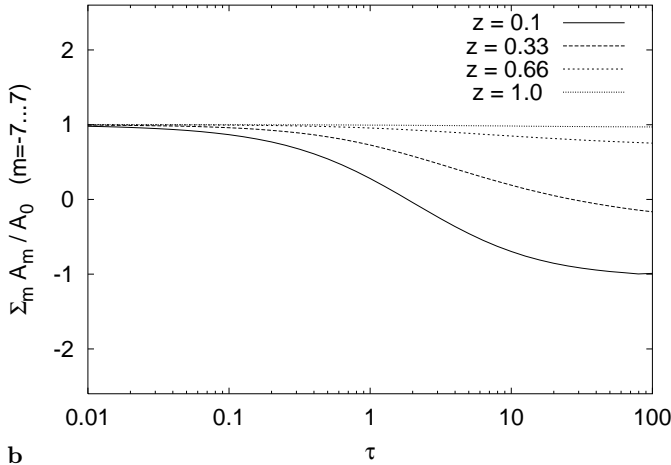
Fig. 3a,b. Comparison of the BFKL amplitude approximated by a partial sum in (37) up to conformal spin $|n| = |2m| = 14$ with the leading conformal spin result, $n = 0$. Dependencies of the ratio are given as a function of **a** z and **b** τ respectively
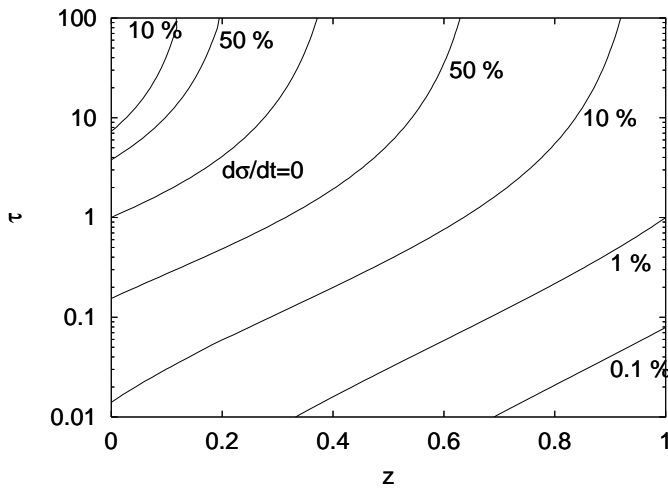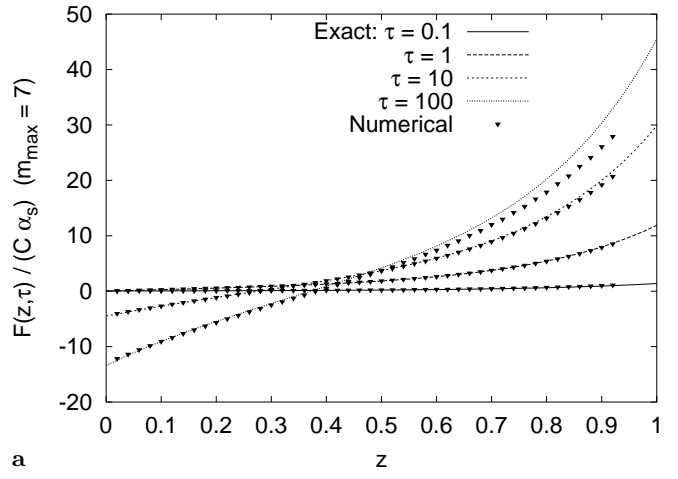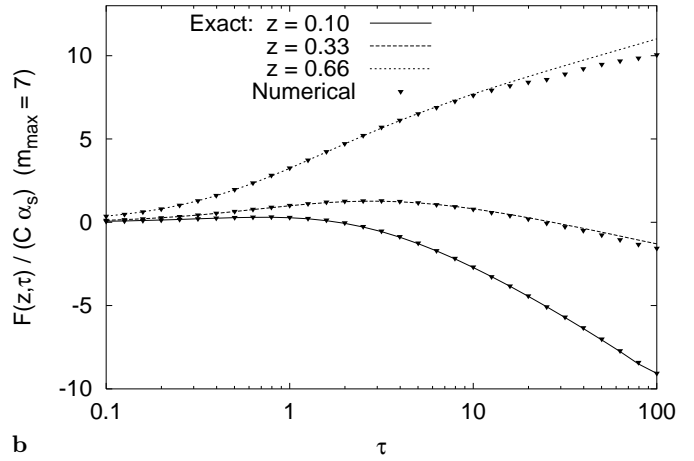

Fig. 4. Contour plot showing the relative error $\mathcal{E}$ of the cross-section obtained in the $n = 0$ approximation to formula (37) in the (z, τ) plane. In this plot $\mathcal{E} < 0$. The contour labelled $d\sigma/dt = 0$ corresponds to values of z and τ for which the exact cross-section vanishes

Fig. 5a,b. Comparison of analytical and numerical results shown as a function of **a** z for various τ **b** τ for various z

those non-leading effects in the analysis. In this case, the conformal symmetry of the kernel is broken and no exact analytical approach is known yet. Fortunately, using the more straightforward numerical method one may obtain a solution to the BFKL equation beyond the leading logarithmic approximation (BFKL LL+NL), given by (16). In Fig. 6 the rapidity $y = \ln(1/x)$ (c.f. (12), (16)) and $|t|$ dependencies of the cross-section $d\sigma/dt\,(y, |t|)$ for J/ψ production off a quark are shown. The cross-sections obtained from the LL BFKL and BFKL LL+NL are compared. At the leading logarithmic accuracy the value of the fixed coupling α_s is not constrained and we choose $\alpha_s = 0.17$. With this choice, the LL and LL+NL results in the studied window of y and $|t|$ have a similar overall normalization. In the BFKL LL+NL equation (16), we take $s_0 = 0.5$ GeV^2, and the scales of the running coupling according to (17). It may be seen in Fig. 6a, that the increase for large y is less steep (i.e. the intercept is smaller) for the LL+NL case, in spite of taking a rather small value of α_s in the LL BFKL equation. To be precise, the pomeron intercept is $\alpha_P = 1.45$ for the LL BFKL curves and $\alpha_P \simeq 1.3$ for the non-leading solution. It is clear, that the non-leading prediction is much closer to the experimental estimates of $\alpha_P \simeq 1.2$ in the vector meson production process.
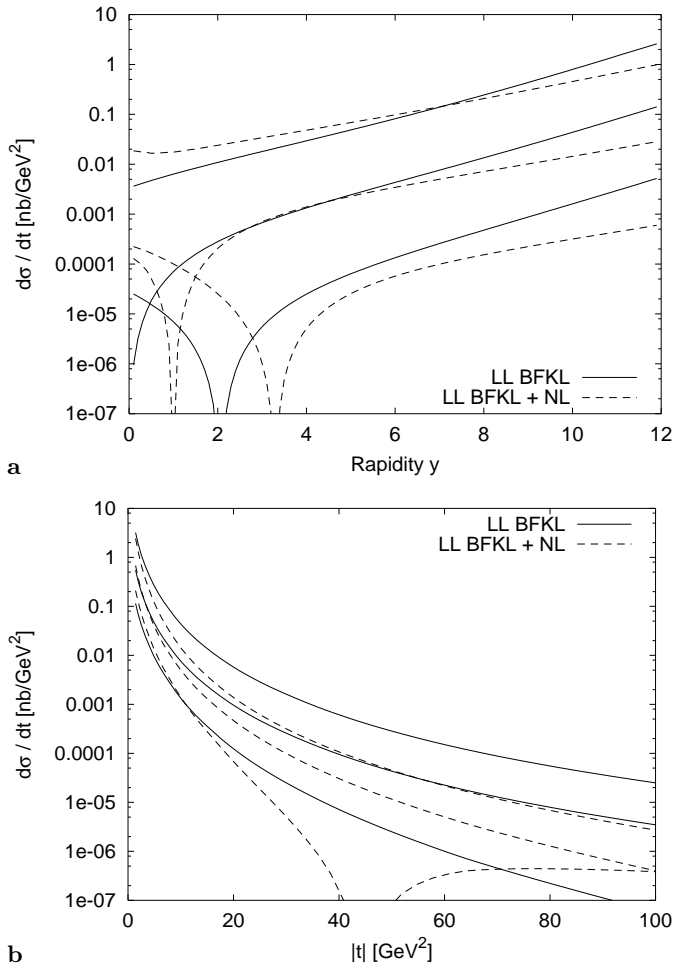
a

b

Fig. 6a,b. The cross-sections $d\sigma/dt(y,|t|)$ for diffractive J/ψ production off a quark shown as a function of **a** rapidity y for $|t| = 3$ GeV^2 (uppermost curves), 10 GeV^2 (in the middle) and 30 GeV^2 (lowermost curves), and **b** momentum transfer $|t|$ for $y = 4$ (lowermost curves), $y = 7$ (in the middle) and $y = 10$ (uppermost curves). Solid curves are obtained from the LL BFKL equation and dashed ones from the BFKL LL+NL equation

Thus, when both the normalization (which also depends on α_s) and the rapidity dependence are taken into account, the need for NL effects in the BFKL kernel should become visible. Comparison of the shapes in $|t|$, given in Fig. 6b, demonstrates that they are similar in both cases, especially in the low $|t|$ range. The LL+NL curves are steeper because of the running of α_s. To conclude, the main impact of the non-leading corrections seems to be a reduction of the pomeron intercept.

6 Comparison with data

The results of the model calculation described in the previous sections may be compared to the ZEUS data [5] on diffractive J/ψ photoproduction. In this measurement, the photon virtuality $Q^2_\gamma \simeq 0$ and the photon-proton collision energy is in the range 80 GeV $< W <$ 120 GeV.
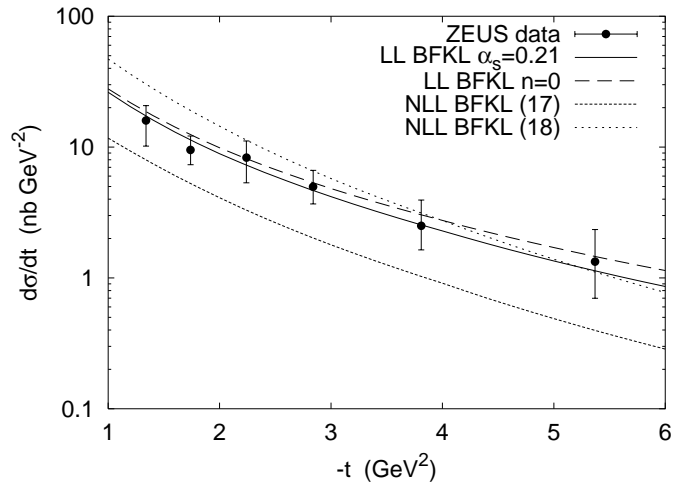

Fig. 7. The cross-section $d\sigma/dt$ for diffractive J/ψ photoproduction off proton shown as a function of the momentum transfer $|t|$. ZEUS data are compared with the theoretical results from: LL BFKL (continuous line), the leading conformal spin approximation to LL BFKL amplitude (dashed line) and the BFKL equation with non-leading corrections (dotted lines where lower and upper lines correspond to the choices of scales given by (17) and (18) respectively). A correlated 10% uncertainty of the normalization of data points is not included into the error bars

In Fig. 7 the data are shown together with the theoretical curves obtained from (1) with various models. These curves were obtained using the CTEQ5L parton distributions [25]. The continuous curve is given by the analytical solution of the BFKL equation (37) with $\alpha_s = 0.21$ and all conformal spins included, and the dashed one corresponds to the leading conformal spin ($n = 2m = 0$) in (37). The dotted curves are obtained from the BFKL equation with non-leading effects (16). For the lower curve, the strong coupling constant in the impact factors is evaluated at the scales given by (17), and for the upper curve we use the values given by (18) as described in Sect. 3.

The LL BFKL results fit the data very well and the difference between the leading conformal spin and the full solution is small, although the discrepancy increases with t. The non-leading BFKL results are in rather good agreement with the data when low scales of α_s are chosen (18), but underestimate the data when the most natural choice (17) of scales is made. Thus, in formulating predictions extrapolating beyond the currently measured kinematical window, we will use the data-guided option (18). We have also checked, that the sensitivity of the normalization of the non-leading BFKL results to the value of s_0 is relatively large within the considered window: for the scale choice (17), it increases by a factor of two when s_0 decreases from 0.5 GeV^2 to 0.1 GeV^2. The t-dependence is only slightly steeper at low t for the latter case. Therefore, the shape of the cross-section is stable against variation of details, while the normalization is more uncertain, and critical tests of BFKL should be based on the shape rather than the normalization of the cross-section.

Recall that an important feature of the non-leading BFKL solution is the emerging value of the pomeron intercept of about 1.3, to be compared with the LL BFKL value $\alpha_P = 1.56$ for $\alpha_s = 0.21$. Thus, we expect that the LL BFKL should overestimate significantly the cross-sections for larger average collision energies W. An interesting experimental verification of the impact of non-leading corrections on the scattering amplitudes could be provided by performing analogous measurements at higher energies W. In Fig. 8 theoretical estimates from LL BFKL and non-leading BFKL are shown for the photon-proton collision energy $W = 100$ and 200 GeV, for a wide t range. The parameters are adjusted to give the best fits of the presently available ZEUS data, that is $\alpha_s = 0.21$ for LL BFKL, $s_0 = 0.5$ GeV^2 and the running coupling being taken at scales (18). One may see that although the inclusion of non-leading corrections lowers the expected value of the cross-sections at $W = 200$ GeV it may be insufficient to discriminate between the models. We have checked that the impact of higher conformal spins may be safely neglected at $W = 200$ GeV and $|t| < 10$ GeV^2.

Note that the cross-sections fall off much steeper with increasing t when the non-leading corrections are included (see Fig. 8 a,b). This is mostly because of the running of the coupling with the energy scale related to the momentum transfer.

7 Conclusions

In this paper an analysis was performed of BFKL amplitudes for diffractive heavy vector meson photoproduction at large momentum transfer. We obtained an explicit complete solution to the leading-logarithmic BFKL equation describing this process. The novel feature of our approach is the inclusion of terms subleading at very high rapidity, corresponding to higher conformal spins in Lipatov's expansion of the BFKL amplitude. These subleading effects were found to reduce theoretical expectations for the cross-sections by about 10% in the kinematical window currently probed by experiments on the J/ψ production. This result gives a firmer ground for the previous results, based on the leading conformal spin approximation. The relative importance of higher conformal spins increases, however, with decreasing collision energy or increasing momentum transfer, as shown in Fig. 4.

Also non-leading corrections to BFKL equations were taken into account phenomenologically by using the running coupling constant and applying the so-called consistency constraint in the BFKL kernel. In this case a numerical method was used to solve the equation. The main influence of non-leading corrections was found to be a reduction of the hard pomeron intercept to about 1.3, close to the value determined from experiment.

Results obtained from both approaches were compared to the experimental data on the t-dependent differential cross-section for J/ψ photoproduction at γp collision energy $W \sim 100$ GeV. In both cases a good fit was obtained, although we found that the cross-section grows much slower with rapidity when non-leading corrections
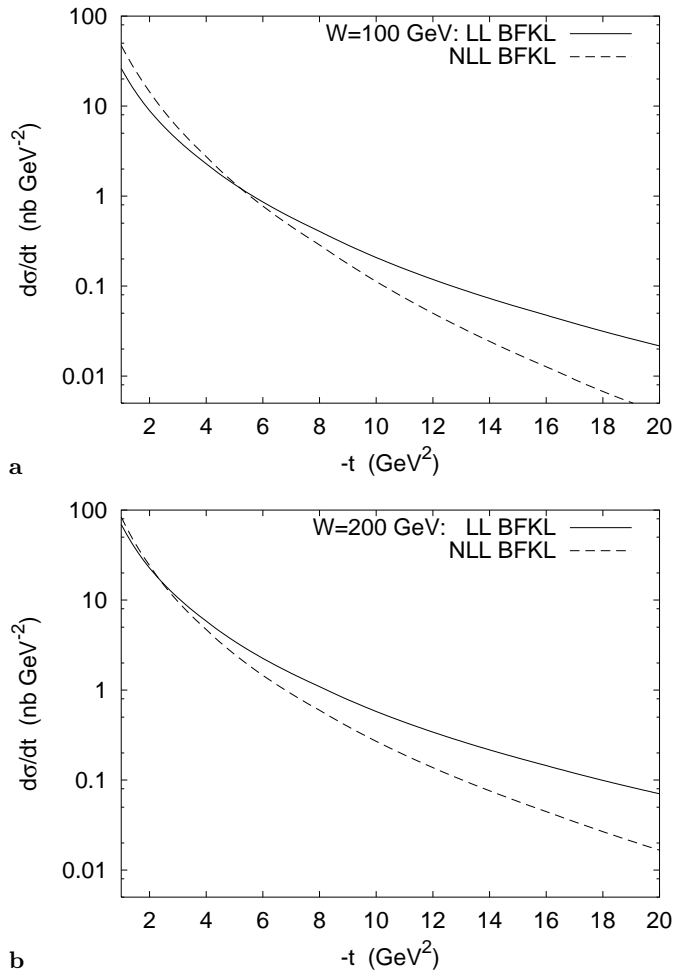

Fig. 8a,b. The cross-sections $d\sigma/dt$ for diffractive J/ψ photoproduction off proton shown as a function of the momentum transfer $|t|$ for γp collision energy **a** $W = 100$ GeV and **b** $W = 200$ GeV. The continuous and dotted lines represent the LL BFKL and BFKL with non-leading corrections results respectively

are included, leading to a discrepancy from the LL BFKL results increasing with rapidity. The ratio of the differential cross-sections at $W = 200$ GeV and $W = 100$ GeV may be used to find the influence of non-leading corrections to the BFKL equation if the data are accurate enough.

To summarize, we provide more insight into the BFKL mechanism of diffractive heavy vector meson production and confirm that the available data are consistent with BFKL expectations.

References

1. L.N. Lipatov, Sov. J. Nucl. Phys. **23**, 338 (1976); E.A. Kuraev, L.N. Lipatov, V.S. Fadin, Sov. Phys. JETP **44**, 443 (1976); ibid. **45**, 199 (1977); I.I. Balitsky, L.N. Lipatov, Sov. J. Nucl. Phys. **28**, 822 (1978)
2. L.N. Lipatov, Sov. Phys. JETP **63**, 904 (1986); Phys. Rep. **286**, 131 (1997)
3. J.R. Forshaw, M.G. Ryskin, Z. Phys. C **68**, 137 (1995)
4. J. Bartels, J.R. Forshaw, H. Lotter, M. Wüsthoff, Phys. Lett. B **375**, 301 (1996)
5. S. Chekanov et al. [ZEUS Collaboration], hep-ex/0205081, Eur. Phys. J. C, in press
6. J.R. Forshaw, G. Poludniowski, hep-ph/0107068, Eur. Phys. J. C, in press
7. A.H. Mueller, W.-K. Tang, Phys. Lett. B **284**, 123 (1992)
8. L. Motyka, A.D. Martin, M.G. Ryskin, Phys. Lett. B **524**, 107 (2002)
9. V.S. Fadin, L.N. Lipatov, Phys. Lett. B **429**, 127 (1998); M. Ciafaloni, G. Camici, Phys. Lett. B **430**, 349 (1998)
10. R. Enberg, G. Ingelman, L. Motyka, Phys. Lett. B **524**, 273 (2002)
11. R. Enberg, J. Forshaw, L. Motyka, G. Poludniowski, in preparation
12. J. Bartels, J.R. Forshaw, H. Lotter, L.N. Lipatov, M.G. Ryskin, M. Wüsthoff, Phys. Lett. B **348**, 589 (1995)
13. J.M. Cornwall, Phys. Rev. D **26**, 1453 (1982); C. Alexandrou, P. de Forcrand, E. Follana, Phys. Rev. D **63**, 094504 (2001)
14. C. Alexandrou, P. de Forcrand, E. Follana, Phys. Rev. D **63**, 094504 (2001); D.B. Leinweber, J.I. Skullerud, A.G. Williams, C. Parrinello [UKQCD collaboration], Phys. Rev. D **58**, 031501 (1998)
15. M.B. Gay Ducati, W.K. Sauter, Phys. Lett. B **521**, 259 (2001)
16. M.G. Ryskin, Z. Phys. C **57**, 89 (1993)
17. L. Frankfurt, W. Koepf, M. Strikman, Phys. Rev. D **57**, 512 (1998)
18. D.Y. Ivanov, R. Kirschner, A. Schäfer, L. Szymanowski, Phys. Lett. B **478**, 101 (2000) [Erratum-ibid. B **498**, 295 (2001)]
19. B. Andersson, G. Gustafson, H. Kharraziha, J. Samuelsson, Z. Phys. C **71**, 613 (1996); J. Kwieciński, A.D. Martin, P.J. Sutton, Z. Phys. C **71**, 585 (1996)
20. G.P. Salam, JHEP **9807**, 019 (1998); M. Ciafaloni, D. Colferai, G.P. Salam, Phys. Rev. D **60**, 114036 (1999); G.P. Salam, Acta Phys. Polon. B **30**, 3679 (1999)
21. J. Kwieciński, A.D. Martin, A.M. Staśto, Phys. Rev. D **56**, 3991 (1997)
22. J. Kwieciński, L. Motyka, Phys. Lett. B **438**, 203 (1998)
23. J. Kwieciński, L. Motyka, Phys. Lett. B **462**, 203 (1999)
24. H. Navelet, R. Peschanski, Nucl. Phys. B **507**, 353 (1997)
25. H.L. Lai et al., Eur. Phys. J. C **12**, 375 (2000)